Published in final edited form as:
Cancer Lett. 2008 September 28; 269(1): 57–66. doi:10.1016/j.canlet.2008.04.026.

Gold nanorod assisted near-infrared plasmonic photothermal therapy (PPTT) of squamous cell carcinoma in mice

Erin B. Dickerson[a,†], **Erik C. Dreaden**[b,†], **Xiaohua Huang**[b,†], **Ivan H. El-Sayed**[c], **Hunghao Chu**[b], **Sujatha Pushpanketh**[b], **John F. McDonald**[a], and **Mostafa A. El-Sayed**[b,*]

[a]School of Biology, Ovarian Cancer Institute, Georgia Institute of Technology, Atlanta, GA 30332

[b]Laser Dynamics Laboratory, School of Chemistry and Biochemistry, Georgia Institute of Technology, Atlanta, GA 30332

[c]Otolaryngology-Head and Neck Surgery, Comprehensive Cancer Center, University of California at San Francisco, CA 94143, USA

Abstract

Plasmonic photothermal therapy (PPTT) is a minimally-invasive oncological treatment strategy in which photon energy is selectively administered and converted into heat sufficient to induce cellular hyperthermia. The present work demonstrates the feasibility of *in vivo* PPTT treatment of deep-tissue malignancies using easily-prepared plasmonic gold nanorods and a small, portable, inexpensive near-infrared (NIR) laser. Dramatic size decreases in squamous cell carcinoma xenografts were observed for direct ($P<0.0001$) and intravenous ($P<0.0008$) administration of pegylated gold nanorods in *nu/nu* mice. Inhibition of average tumor growth for both delivery methods was observed over a 13-day period, with resorption of >57% of the directly-injected tumors and 25% of the intravenously-treated tumors.

Keywords

nanotechnology; photothermal therapy; nanorod; hyperthermia; near infrared; polyethylene glycol

1. Introduction

The application of nanotechnology in medicine has been a rapidly growing field in recent years [1–8]. A variety of structures with unique structural [9, 10], optical [11, 12], electronic [13], magnetic [14], and catalytic [15] properties have been exploited in the areas of cancer imaging [2, 16–19], diagnostics [6, 20, 21], and treatment [22–30]. Noble metal nanoparticles provide remarkable opportunities in these applications due to their inherently

*Corresponding author. Mostafa A. El-Sayed: mostafa.el-sayed@chemistry.gatech.edu. 901 Atlantic Dr NW, Atlanta, GA 30332-0400 Tel: 404-894-0292. Fax: 404-894-0294.
†equal contribution by EBD, ECD, and XH.

Supporting Information
Observed changes in HSC-3 xenograft growth for intratumoral nanorod injections in female *nu/nu* mice without NIR exposure, NIR exposure alone, and PBS intratumoral injections alone ($P=0.427$ at day 9) (S1). S2 illustrates representative tumor resorption and growth inhibition following direct injection of pegylated gold nanorods and near-infrared PPTT versus sham/NIR treatments. Change in tumor volume for individual mice following established conditions for near-infrared PPTT treatment of HSC-3 xenografts by control (a), intravenous (b), and direct (c) injections of pegylated gold nanorods (S3).

low toxicity [31–33] and strongly enhanced optical properties associated with localized surface plasmon resonance [34–36]. The enhanced electromagnetic field surrounding such particles gives rise to large absorption, Rayleigh (Mie) scattering, raman scattering, and two-photon luminescence cross-sections, properties which have been utilized in photothermal cancer therapy [24–30] (PTT), surface enhanced Raman detection [37–39] (SERS), and diagnostic imaging [17–20] applications.

While surgical excision of tumors is a highly effective method of cancer treatment, curative strategies for primary tumors located in vital or poorly accessible tissues remains a challenge. In cases of recurrent tumors or those with ill-defined margins, alternative and multimodal oncological approaches are employed. The primary [40–42] and adjunctive [43–46] treatment of cancers by induced hyperthermia is a well established but burgeoning field of medical research. Here, temperatures in tumor-loaded tissues are elevated to 40–43°C [47] and above by selective or non-selective application of microwave, radio, ultrasound, alternating magnetic, infrared, or visible radiation. At temperatures greater than 43°C, protein denaturation and disruption of the cellular membrane is known to occur and ablation of tumor tissues has been shown in numerous cases [42, 48, 49]. Under mild temperature increases, clinical studies indicate an acceleration in both perfusion and reoxygenation [50, 51] of tumor tissues, thereby increasing the efficacy of cytostatic drug delivery (*chemosensitization*) and radiotherapy (*radiosensitization*), respectively. In all cases, clinical studies indicate statistically significant benefits to local tumor control and overall survival rates for primary [40–42] and conjunctive hyperthermia [52–56]. Although promising, conventional non-invasive hyperthermic strategies are often less selective than those based-on or used in combination with thermal contrast agents, in many cases, causing damage to surrounding healthy tissues, as well as significant discomfort. Moreover, hyperthermic treatments using commercially available instruments are often limited to shallow penetration depths [46] (<3 cm), lower treatment temperatures, and regions of the body with regular surface composition. Invasive approaches using microwave antennas are highly susceptible to interference, while magnetic particle treatments require large doses.

Photothermal therapy [49, 57–59] is a minimally-invasive treatment method in which photon energy is converted to thermal energy sufficient to induce cellular hyperthermia. Selectivity is achieved by focused directional control or invasive [40–42] (fiber optic) positioning of the incident radiation, often pulsed [28–30] or continuous wave [24–28, 30, 48] (cw) laser, and is typically accompanied by preferential administration of photoactive molecules [60–62] or nano-scale particles. Photoexcitation of the latter two results in non-radiative relaxation by local heat transfer to the surrounding tumor environment. In contrast, photodynamic therapy [63–65] (PDT), relies on non-radiative relaxation through local formation of cytotoxic singlet oxygen species. While PTT and PDT treatments have garnered significant attention, such methods are inherently limited by photobleaching effects and absorption cross sections several times weaker than those of noble metal nanoparticles.

Recent advances in the field of plasmonics present new opportunities for both primary and multimodal PTT strategies using noble metal nanoparticles. By photo-exciting conduction electrons which oscillate at the surfaces of such structures (surface plasmons), highly efficient local heating can be achieved by non-radiative relaxation through electron-phonon and subsequent phonon-phonon coupling processes [35]. While several materials and spherical nanoparticles exhibit surface plasmon resonance in the visible region, opportunities for *in vivo* plasmonic photothermal therapy [8] (PPTT) are restricted due to a high degree of absorption by tissues at visible wavelengths. Such ablative treatments are therefore limited to shallow depths [66]. In contrast, PPTT of deep tissue malignancies may be accomplished by laser exposure and plasmon absorption in the near-infrared region (NIR). Due to minimal attenuation by water and hemoglobin at these wavelengths, NIR

transmission [7] in soft tissues may be achieved at depths exceeding 10 cm. By chemically varying the shape or composition of noble metal nanoparticles [9, 21, 24, 67–69], surface plasmon absorption can be tuned from ultraviolet (UV) to infrared (IR) wavelengths. The enhanced nonlinear optical properties of spherical metal nanoparticles have also been used by our group in *in vitro* near-infrared pulsed laser PPTT by second harmonic generation [29, 70, 71].

The potential uses of gold nanoparticles in near-infrared PPTT have been published using a variety of noble metal nanostructures, including gold nanoshells [26, 48], gold nanorods [8, 27, 72], and recently, gold nanocages [73]. Studies using nanoshell-mediated PPTT indicate significantly improved local tumor control and survival times in animal models, while surface plasmon absorption of gold nanocages have been used in diagnostic imaging and *in vitro* therapy [24].

One of the simplest and widely used methods to obtain plasmonic nanoparticles involves the seed-mediated growth of colloidal gold nanorods [68]. The use of such particles in near-infrared PPTT is highly attractive due to their rapid synthesis, facile bioconjugation, strong absorption cross-section, and tunable optical extinction. Recent calculations by discrete dipole approximation (DDA) show the absorption cross section of nanorod structures to be nominally larger than that of nanocages and more than twice that of nanoshell structures at their NIR plasmon resonance [73]. By synthetically varying the aspect ratio of the nanorods, longitudinal plasmon absorption can be shifted throughout the visible, NIR, and IR regions [68, 74–76].

Our previous work [27] showed that gold nanorods conjugated to epithelial growth factor receptor antibodies (anti-EGFR) can serve as contrast agents for *in vitro* biodiagnostics. Moreover, due to overexpression of the EGF receptor on cancer cell surfaces and the specificity of antibody binding, malignant cells were found to require half the energy necessary to destroy normal cells when both were incubated with the same concentration of nanorod bioconjugates, a key feature of selective PPTT.

In the present work, the feasibility of *in vivo* near-infrared PPTT is demonstrated using colloidal gold nanorods in an animal model. Subcutaneous squamous cell carcinoma xenografts were grown in nude (*nu/nu*) mice and particles were selectively delivered to tumors by both direct and intravenous injection. Thiolated poly (ethylene) glycol (PEG5000) was covalently bound to the gold nanorod surface to increase biocompatibility [77–80], suppress immunogenic responses, and to decrease adsorption to the negatively charge luminal surface of blood vessels. Near-infrared PPTT was performed extracorporally using a small, portable, inexpensive, continuous wave diode laser. Making use of the enhanced permeability and retention (EPR) effect [81, 82], preferential accumulation of peylgated gold nanorods in tumor tissues was achieved due to the high density, extensive extravasation, and inherently defective architecture of the tumor vasculature, as well the diminished lymphatic clearance from associated interstitial spaces. Significant decreases in tumor growth were observed for both direct tumor injection ($P<0.0001$) and intravenous ($P<0.0008$) treatments. Inhibition of average tumor growth for both delivery methods was observed over a 13-day period, with resorption of >57% of the directly-injected tumors and 25% of the intravenously-treated tumors.

2. Materials and Methods

2.1. Synthesis and pegylation of gold nanorods

Seed-mediated growth was performed at 25 °C from freshly prepared aqueous solutions (18 MΩ) following methods of Nikoobakht and El-Sayed [68]. Briefly, 2.50 mL of 1.00 mM

$HAuCl_4$ (Aldrich, 24459-7) was added to 5.00 mL of 0.200 M cetyltrimethylammonium bromide (CTAB, Aldrich). 600 μL of ice-cold 10 mM $NaBH_4$ (Aldrich, 480886) was added to the stirred solution and allowed to react for several minutes, forming the pale brown gold seed solution. Next, 100.0 mL of 1.00 mM $HAuCl_4$ was added to 100.0 mL of 0.200 M CTAB and 4.50 mL of 4.00 mM $AgNO_3$ (Fischer). 1.40 mL of 78.8 mM ascorbic acid (Aldrich, A-7506) was added, followed by gentle mixing to form the transparent growth solution. 160 μL of the seed solution was added to the unstirred growth solution and allowed to react for 2 hours. Nanorods synthesized by this method are approximately 12 nm in width and 50 nm length (4.0 aspect ratio), with a longitudinal plasmon absorption maximum at 800 nm.

Gold nanorods solutions were centrifuged twice at 20,000 × *g* for 15 min and re-dispersed in deionized water to remove excess CTAB molecules. mPEG-SH (Nektar Therapeutics, MW5000) was added to the ~1 nM colloidal nanorod solution at a final concentration of 10 mM. Rods were sonicated overnight and centrifuged at 20,000 × *g* for 15 min and redispersed in deionized water to remove non-specifically bound PEG molecules. The pegylated gold nanorods were again centrifuged at 20,000 × *g* for 15 min, sterile filtered, and re-dispersed in 10 mM phosphate-buffered saline (PBS, Mediatech) to the desired optical density at 800 nm. Extinction spectra of the pegylated nanorod saline suspensions showed no peak shift, broadening, or reduction over a 1 week period prior to injection.

2.2. Cell culture and inoculation of mice with tumor cells

HSC-3 human squamous carcinoma cells were cultured in DMEM (Mediatech) supplemented with 10% v/v heat-inactivated fetal bovine serum (Invitrogen), 2 mM L-glutamine (Sigma), penicillin (100 U/ml) (Sigma), and streptomycin (100 μg/ml) (Sigma) in a 5% CO_2 humidified atmosphere. Female *nu/nu* mice, 7–8 weeks of age, were obtained from Taconic (Hudson, NY). Mice were injected subcutaneously in the flank with 100 μL (3×10^6) HSC-3 cells suspended in 10 mM PBS. Near-infrared PPTT began once tumor burden reached 3 mm in diameter (7–9 days). All experiments were conducted with the approval of the Institutional Animal Care and Use Committee (IACUC) of the Georgia Institute of Technology (Atlanta, GA).

2.3. Intratumoral nanoparticle accumulation, temperature, and imaging

Tumor bearing mice were injected with gold nanorods ($OD_{\lambda=800}$ = 120, 100 μl) via the tail vein, and euthanized at specified time points. Tumor tissues was excised, fixed in 10% formalin for 24 hours, and embedded in paraffin blocks. Blocks were sectioned (5 microns) and stained using the Silver Enhancer Kit SE-100 (Sigma-Aldrich) according to the manufacturer's instructions. Incubation time for optimal visualization was determined to be 10 minutes. Silver staining of the tissue sections were examined using a BX60 Olympus microscope, and photographed using an Olympus Camedia digital camera.

Thermal transient measurements of HSC-3 tumor interstitia were obtained using a 33 gauge hypodermic thermocouple (Omega). The tip of the thermistor was positioned at the tumor center-of-mass and temperatures were recorded in 15 second intervals prior to, during, and following NIR exposure for direct (15 μL, $OD_{\lambda=800}$=40, 10 min, 0.9–1.1 W/cm^2, 6 mm dia) and intravenously (100 μL, $OD_{\lambda=800}$=120, 10 min, 1.7–1.9 W/cm^2, 6 mm dia) administered gold nanorods, as well as for comparably exposed sham/NIR treatments (15 μL direct intratumoral injection of 10 mM PBS).

In vivo imaging of pegylated gold nanorod accumulation was monitored by attenuation of near-infrared transmission (808 nm diode laser, Power Technologies) using a custom-built CCD device array. Control measurements were taken from images obtained by 15 μL direct

intratumoral injection of 10 mM PBS, while directly and intravenously administered measurements were obtained using previously mentioned dosages.

2.6. In vivo near-infrared PPTT

Mice were anesthetized with ketamine/xylazine/acepromazine. 15 μL of pegylated gold nanorods ($OD_{\lambda=800}$ = 40) were directly injected into the tumor interstitium or 100 μL of pegylated gold nanorods ($OD_{\lambda=800}$ = 120) were intravenously (tail) injected. Control tumor sites were injected with 15 μL of 10 mM PBS with no NIR exposure. For direct administration, mouse tumors were extracorporeally exposed to NIR radiation (0.9–1.1 W/cm^2, 6 mm dia, 10 min) within 2 minutes of injection to limit particle diffusion beyond the tumor boundaries. For intravenous administration, nanorods were allowed 24 hour circulation to maximize intratumoral particle accumulation prior to NIR exposure (1.7–1.9 W/cm^2, 6 mm dia,10 min). Ellipsoidal tumor volume was calculated as $V = (d)^2(D)(\pi/6)$. Statistical hypothesis testing was performed using Welch's t test and non-parametric analysis of variance was performed by the Kruskal-Wallis test. Due to the unusually rapid growth rates observed in the HSC-3 xenograft model, tumors and vital organs were harvested at day 14 for use in separate, ongoing toxicological investigations.

3. Results and Discussion

3.1. Intratumoral particle accumulation

Pegylated gold nanorods were intravenously injected (tail vein) to assess optimal intratumoral particle accumulation. Following injection, HSC-3 tumors were excised at varying time intervals, fixed, sectioned, and stained with silver to visualize the extent of particle loading. Nanorods directly injected into tumors were used for as a positive control (data not shown). Fig. 1a shows a typical histological section from a HSC-3 tumor injected with 15 μL of 10 mM PBS (control). Fig. 1b and 1c illustrate representative tumor sections following 2 and 6 hours of accumulation, respectively. At these time points, no appreciable accumulation of particles was observed. In contrast, high particle loading was observed following 24 hours of circulation (Fig. 1d). Because the highest accumulation, and therefore PPTT selectivity, was observed at 24 hours, this time point was used for subsequent intravenous near-infrared PPTT treatments.

Transient particle accumulation following direct and intravenous administration was monitored by NIR transmission imaging (Fig. 2). Intensity line-scans of NIR extinction showed marginal diffusion of directly injected particles over 3 min, with no subsequent change observed over several hours. Intensity line-scans from NIR transmission images of HSC-3 tumor sites directly injected with 15 μL of 10 mM PBS show nominal extinction due to increased tissue density, while line-scans obtained following intravenous nanorod delivery at 24 hr accumulation showed extinction 2.00 times that observed for control sites. Directly injected tumor sites showed NIR extinction at 2 min nanorod diffusion more 2.18 times that observed by intravenous administration and 4.35 times that observed at control sites.

3.2 Thermal response measurements and nanorod accumulation

Thermal transient measurements for direct (Fig. 3a) and intravenous (Fig. 3b) near-infrared PPTT treatments show thermal equilibrium conditions prior to NIR irradiation. Rapid heating was observed upon exposure, followed by steady-state equilibrium. Note that >90% of the observed temperature increase occurred within the first 3 minutes. Upon removal of NIR exposure, tissues displayed expected Newtonian cooling behavior.

Heating efficiencies of PPTT treatments (the ratio of steady-state temperature change in the presence of plasmonic particles to that NIR exposed in their absence) were found to be 3.59±0.5 for direct-injection and 1.90±0.4 for intravenous injection of pegylated gold nanorods. The former value is remarkably similar to that observed during *in vivo* near-infrared PPTT treatments reported by Hirsch et al.[26] by direct injection of gold nanoshells. Observed increases in temperature change for sham/NIR treatments using comparable exposure times and power densities as direct and intravenous administration conditions correlate well with increases in power density. Disparity of direct and intravenous PPTT heating efficiency scales proportionately with observed increases in NIR extinction (4.35 and 2.00 times greater than control extinction, respectively) and is attributed to decreased particle loading by intravenous delivery. Although particle volume and concentration was significantly higher for intravenous injections, accumulation is likely limited by the extent of tumor angiogenesis and uptake by the reticuloendothelial system (RES). Treatment selectivity and efficacy was most apparent for direct injections; however, both methods showed significantly improved local tumor control.

3.3 Tumor growth suppression: direct versus intravenous injection

Groups of four to six mice were initially used to establish optimal conditions for near-infrared PPTT treatment of HSC-3 tumor xenografts. 15 μl of pegylated gold nanorods ($OD_{\lambda=800}$=40) were directly administered at three sites within the tumor interstitium or 100 μL ($OD_{\lambda=800}$=120) were intravenously injected (tail). After two minutes, tumors directly injected with nanorods were subjected to extracorporeal NIR exposure (808 nm, 6 mm dia) and it was determined that 10–15 minutes of irradiation at 0.9–1.1 W/cm^2 was necessary for maximal tumor control and minimal damage to surrounding tissues. After 24 hours, tumors intravenously administered with nanorods were also subjected to extracorporeal NIR exposure (808 nm, 6 mm dia) and it was determined that 10–15 minutes of irradiation at 1.7–1.9 W/cm^2 was necessary for maximal tumor control and minimal damage to surrounding tissues. In addition, no statistically significant differences in tumor growth were observed for direct nanorod injections without NIR exposure, sham/NIR exposure alone, and PBS intratumoral injections alone (P=0.427 at day 9) (S1). S2 illustrates typically observed tumor resorption and growth inhibition following direct injection of pegylated gold nanorods and near-infrared PPTT versus sham/NIR treatments.

Using previously established treatment conditions, change in tumor volume was recorded over a 13 day period for control mice, as well as those treated by intravenous and direct nanorod injections followed by PPTT (S3). Here, control mice were subjected to 15 μL direct injection of 10 mM PBS to the tumor interstitium, with no NIR exposure. Average change in tumor volume for each group was plotted (Fig. 4) and statistical hypothesis testing for differences in average tumor growth was performed (Table I). Figure 4 shows a >96% decrease in average tumor growth for directly treated HSC-3 xenografts and a >74% decrease in average tumor growth for intravenously treated HSC-3 xenografts at day 13 (relative to control tumors). Moreover, resorption of >57% of the directly treated tumors and 25% of the intravenously treated tumors was observed over the monitoring period.

Average tumor growth at day 13 for directly and intravenously treated tumors was significantly less than that observed in untreated control groups (P<0.0001 and P<0.0008, respectively). Differences in observed efficacy for direct and intravenous treatments gradually increased during the experiment, reaching statistical significance at the 8% level on day 13. Non-parametric analysis of variance for the treated and untreated groups (Table II) found statistically significant differences at the 2% level and below for the duration of the experiment. These results clearly indicate both the selectivity and specificity of near-infrared PPTT.

The dramatic changes in observed HSC-3 tumor growth are attributed to selective hyperemia of malignant tissues treated with pegylated gold nanorods by near-infrared PPTT. Preferential accumulation of pegylated gold nanorods within the tumor interstitium occurs due to the EPR effect [81]. Because of their rapid metabolic rates, tumor cells are regarded as increasingly vulnerable to hyperthermic effects [44, 72] such as disruption of metabolic signaling processes, protein denaturation, and the onset of acidosis or apoptosis caused by the production of heat-shock proteins [83] and other immunostimulants. Small increases in local temperature are known to result in disruption of nuclear and cytoskeletal assemblies and indeed, previous [44, 84] and recent reports [29, 72] indicate significant membrane blebbing [85–87] under hyperthermic conditions. Under severe conditions, hyperthermic damage can result in impaired vasculature supply, endothelial swelling [44], and mictothrombosis associated with homeostatic disruption [88]. *In vitro,* mild hyperthermia has been shown to impede the function of cell surface receptors, membrane transport, and RNA- and DNA-polymerization during protein synthesis. Repair of sublethal cell damage by DNA-polymerase-α and -β, such as that by incurred during radiotherapy, has also been shown to be inhibited by hyperthermia. While tumor growth suppression and resorption is likely a cumulative result of the previously mentioned effects, it is presumed here that ablation of the tumor vasculature and localized membrane disruption predominates.

Although the mechanism of cellular response in the present case is yet to be determined, the specificity of hyperthermic effects on tumor growth from both direct and intravenous near-infrared PPTT treatments is unmistakable ($P<0.0001$ and $P<0.0008$, respectively). Inhibition of average tumor growth and minimal damage to surrounding tissues is observed for both methods. Resorption of >57% of the directly-injected tumors and 25% of the intravenously-treated tumors clearly indicates the potential curative and adjunctive applications of NIR plasmonic photothermal therapy (PPTT) in pre-clinical settings.

Supplementary Material

Refer to Web version on PubMed Central for supplementary material.

Acknowledgments

The authors graciously thank Mariam Akhtar (GT Dept of Biology) for her assistance with silver staining studies. Generous support from the Georgia Cancer Coalition (EBD; Distinguished Cancer Scientist Award), the National Cancer Institute (MAE, ECD, & XH; Center of Cancer Nanotechnology Excellence Award U54CA119338), the Robinson Family Foundation (JFM), Ovarian Cycle (JFM), Golfers Against Cancer (JFM), and the US Dept of Energy (MAE, ECD, & XH; NO:DE-FG02-97 ER14799) is acknowledged.

References

1. Ferrari M. Cancer nanotechnology: Opportunities and challenges. Nat Rev Cancer. 2005; 5:161–171. [PubMed: 15738981]
2. Gao XH, Cui YY, Levenson RM, Chung LWK, Nie SM. In vivo cancer targeting and imaging with semiconductor quantum dots. Nat Biotechnol. 2004; 22:969–976. [PubMed: 15258594]
3. Katz E, Willner I. Integrated nanoparticle-biomolecule hybrid systems: Synthesis, properties, and applications. Angew Chem Int Edit. 2004; 43:6042–6108.
4. Moghimi SM, Hunter AC, Murray JC. Long-circulating and target-specific nanoparticles: Theory to practice. Pharmacol Rev. 2001; 53:283–318. [PubMed: 11356986]
5. Niemeyer CM. Nanoparticles, proteins, and nucleic acids: Biotechnology meets materials science. Angew Chem-Int Edit. 2001; 40:4128–4158.
6. Rosi NL, Mirkin CA. Nanostructures in biodiagnostics. Chem Rev. 2005; 105:1547–1562. [PubMed: 15826019]

7. Weissleder R. A clearer vision for in vivo imaging. Nat Biotechnol. 2001; 19:316–317. [PubMed: 11283581]
8. Huang X, Jain PK, El-Sayed IH, El-Sayed MA. Gold nanoparticles and nanorods in medicine: From cancer diagnostics to photothermal therapy. Nanomedicine. 2007; 2:681–693. [PubMed: 17976030]
9. Burda C, Chen XB, Narayanan R, El-Sayed MA. Chemistry and properties of nanocrystals of different shapes. Chem Rev. 2005; 105:1025–1102. [PubMed: 15826010]
10. Liz-Marzan LM. Tailoring surface plasmons through the morphology and assembly of metal nanoparticles. Langmuir. 2006; 22:32–41. [PubMed: 16378396]
11. Noguez C. Surface plasmons on metal nanoparticles: The influence of shape and physical environment. J Phys Chem C. 2007; 111:3806–3819.
12. Pileni MP. Self-assembly of inorganic nanocrystals: Fabrication and collective intrinsic properties. Accounts Chem Res. 2007; 40:685–693.
13. Adams DM, Brus L, Chidsey CED, Creager S, Creutz C, Kagan CR, Kamat PV, Lieberman M, Lindsay S, Marcus RA, Metzger RM, Michel-Beyerle ME, Miller JR, Newton MD, Rolison DR, Sankey O, Schanze KS, Yardley J, Zhu XY. Charge transfer on the nanoscale: Current status. J Phys Chem B. 2003; 107:6668–6697.
14. Thomas L, Lionti F, Ballou R, Gatteschi D, Sessoli R, Barbara B. Macroscopic quantum tunnelling of magnetization in a single crystal of nanomagnets. Nature. 1996; 383:145–147.
15. Daniel MC, Astruc D. Gold nanoparticles: Assembly, supramolecular chemistry, quantum-size-related properties, and applications toward biology, catalysis, and nanotechnology. Chem Rev. 2004; 104:293–346. [PubMed: 14719978]
16. Huh YM, Jun YW, Song HT, Kim S, Choi JS, Lee JH, Yoon S, Kim KS, Shin JS, Suh JS, Cheon J. In vivo magnetic resonance detection of cancer by using multifunctional magnetic nanocrystals. J Am Chem Soc. 2005; 127:12387–12391. [PubMed: 16131220]
17. Durr NJ, Larson T, Smith DK, Korgel BA, Sokolov K, Ben-Yakar A. Two-photon luminescence imaging of cancer cells using molecularly targeted gold nanorods. Nano Lett. 2007; 7:941–945. [PubMed: 17335272]
18. Sokolov K, Follen M, Aaron J, Pavlova I, Malpica A, Lotan R, Richards-Kortum R. Real-time vital optical imaging of precancer using anti-epidermal growth factor receptor antibodies conjugated to gold nanoparticles. Cancer Res. 2003; 63:1999–2004. [PubMed: 12727808]
19. Wang H, Huff TB, Zweifel DA, He W, Low PS, Wei A, Cheng JX. In vitro and in vivo two-photon luminescence imaging of single gold nanorods. Proc Natl Acad Sci USA. 2005; 102:15752–15756. [PubMed: 16239346]
20. El-Sayed IH, Huang X, El-Sayed MA. Surface plasmon resonance scattering and absorption of anti-EGFR antibody conjugated gold nanoparticles in cancer diagnostics: applications in oral cancer. Nano Lett. 2005; 5:829–834. [PubMed: 15884879]
21. Loo C, Lowery A, Halas NJ, West JL, Drezek R. Immunotargeted nanoshells for integrated cancer imaging and therapy. Nano Lett. 2005; 5:709–711. [PubMed: 15826113]
22. Johannsen M, Gneveckow U, Eckelt L, Feussner A, Waldofner N, Scholz R, Deger S, Wust P, Loening SA, Jordan A. Clinical hyperthermia of prostate cancer using magnetic nanoparticles: Presentation of a new interstitial technique. Int J Hyperthermia. 2005; 21:637–647. [PubMed: 16304715]
23. Kam NWS, O'connell M, Wisdom JA, Dai HJ. Carbon nanotubes as multifunctional biological transporters and near-infrared agents for selective cancer cell destruction. Proc Natl Acad Sci USA. 2005; 102:11600–11605. [PubMed: 16087878]
24. Chen J, Wang D, Xi J, Au L, Siekkinen A, Warsen A, Li ZY, Zhang H, Xia Y, Li X. Immuno gold nanocages with tailored optical properties for targeted photothermal destruction of cancer cells. Nano Lett. 2007; 7:1318–1322. [PubMed: 17430005]
25. El-Sayed IH, Huang X, El-Sayed MA. Selective laser photo-thermal therapy of epithelial carcinoma using anti-EGFR antibody conjugated gold nanoparticles. Cancer Lett. 2006; 239:129–135. [PubMed: 16198049]
26. Hirsch LR, Stafford RJ, Bankson JA, Sershen SR, Rivera B, Price RE, Hazle JD, Halas NJ, West JL. Nanoshell-mediated near-infrared thermal therapy of tumors under magnetic resonance guidance. Proc Natl Acad Sci USA. 2003; 100:13549–13554. [PubMed: 14597719]

27. Huang X, El-Sayed IH, El-Sayed MA. Cancer cell imaging and photothermal therapy in the near-infrared region by using gold nanorods. J Am Chem Soc. 2006; 128:2115–2120. [PubMed: 16464114]
28. Pitsillides CM, Joe EK, Wei X, Anderson RR, Lin CP. Selective cell targeting with light-absorbing microparticles and nanoparticles. Biophys J. 2003; 84:4023–4032. [PubMed: 12770906]
29. Tong L, Zhao Y, Huff TB, Hansen MN, Wei A, Cheng JX. Gold Nanorods Mediate Tumor Cell Death by Compromising Membrane Integrity. Adv Mater. 2007; 19:3136–3141. [PubMed: 19020672]
30. Zharov VP, Galitovsky VV, Viegas M. Photothermal detection of local thermal effects during selective nanophotothermolysis. Appl Phys Lett. 2003; 83:4897–4899.
31. Connor EE, Mwamuka J, Gole A, Murphy CJ, Wyatt MD. Gold nanoparticles are taken up by human cells but do not cause acute cytotoxicity. Small. 2005; 1:325–327. [PubMed: 17193451]
32. Khan JA, Pillai B, Das TK, Singh Y, Maiti S. Molecular effects of uptake of gold nanoparticles in HeLa cells. Chembiochem. 2007; 8:1237–1240. [PubMed: 17569092]
33. Shukla R, Bansal V, Chaudhary M, Basu A, Bhonde RR, Sastry M. Biocompatibility of gold nanoparticles and their endocytotic fate inside the cellular compartment: A microscopic overview. Langmuir. 2005; 21:10644–10654. [PubMed: 16262332]
34. El-Sayed MA. Some interesting properties of metals confined in time and nanometer space of different shapes. Accounts Chem Res. 2001; 34:257–264.
35. Link S, El-Sayed MA. Shape and size dependence of radiative, non-radiative and photothermal properties of gold nanocrystals. Int Rev Phys Chem. 2000; 19:409–453.
36. Mie G. Contribution to the optics of turbid media, especially colloidal metal suspensions. Ann Phys. 1908; 25:377–445.
37. Huang X, El-Sayed IH, Qian W, El-Sayed MA. Cancer Cells Assemble and Align Gold Nanorods Conjugated to Antibodies to Produce Highly Enhanced, Sharp and Polarized Surface Raman Spectra: A Potential Cancer Diagnostic Marker. Nano Lett. 2007; 7:1591–1597. [PubMed: 17474783]
38. Moskovits M. Surface-Enhanced Spectroscopy. Rev Mod Phys. 1985; 57:783–826.
39. Stuart DA, Yuen JM, Lyandres NSO, Yonzon CR, Glucksberg MR, Walsh JT, Van Duyne RP. In vivo glucose measurement by surface-enhanced Raman spectroscopy. Anal Chem. 2006; 78:7211–7215. [PubMed: 17037923]
40. Amin Z, Donald JJ, Masters A, Kant R, Steger AC, Bown SG, Lees WR. Hepatic Metastases - Interstitial Laser Photocoagulation with Real-Time Us Monitoring and Dynamic Ct Evaluation of Treatment. Radiology. 1993; 187:339–347. [PubMed: 8475270]
41. Eichler K, Mack MG, Straub R, Engelmann K, Zangos S, Woitaschek D, Vogl TJ. Oligonodular hepatocellular carcinoma (HCC): MR-guided laser-induced thermotherapy (LITT). Radiologe. 2001; 41:915–922. [PubMed: 11715583]
42. Nolsoe CP, Torppedersen S, Burcharth F, Horn T, Pedersen S, Christensen NEH, Olldag ES, Andersen PH, Karstrup S, Lorentzen T, Holm HH. Interstitial Hyperthermia of Colorectal Liver Metastases with a Us-Guided Nd-Yag Laser with a Diffuser Tip - a Pilot Clinical-Study. Radiology. 1993; 187:333–337. [PubMed: 8475269]
43. Falk MH, Issels RD. Hyperthermia in oncology. Int J Hyperthermia. 2001; 17:1–18. [PubMed: 11212876]
44. Hildebrandt B, Wust P, Ahlers O, Dieing A, Sreenivasa G, Kerner T, Felix R, Riess H. The cellular and molecular basis of hyperthermia. Critical Reviews in Oncology Hematology. 2002; 43:33–56.
45. Horsman MR, Overgaard J. Hyperthermia: a potent enhancer of radiotherapy. Clinical Oncology. 2007; 19:418–426. [PubMed: 17493790]
46. Wust P, Hildebrandt B, Sreenivasa G, Rau B, Gellermann J, Riess H, Felix R, Schlag PM. Hyperthermia in combined treatment of cancer. Lancet Oncol. 2002; 3:487–497. [PubMed: 12147435]
47. Dewey WC. Arrhenius Relationships from the Molecule and Cell to the Clinic. Int J Hyperthermia. 1994; 10:457–483. [PubMed: 7963805]
48. O'neal DP, Hirsch LR, Halas NJ, Payne JD, West JL. Photothermal Tumor Ablation in mice using near infrared absorbing nanoshells. Cancer Lett. 2004; 209:171–176. [PubMed: 15159019]

49. Sultan RA. Tumour ablation by laser in general surgery. Lasers Med Sci. 1990; 5:185–193.
50. Rau B, Wust P, Tilly W, Gellermann J, Harder C, Riess H, Budach V, Felix R, Schlag PM. Preoperative radiochemotherapy in locally advanced or recurrent rectal cancer: Regional radiofrequency hyperthermia correlates with clinical parameters. Int J of Radiat Oncol Biol Phys. 2000; 48:381–391. [PubMed: 10974451]
51. Song CW, Shakil A, Osborn JL, Iwata K. Tumour oxygenation is increased by hyperthermia at mild temperatures. Int J Hyperthermia. 1996; 12:367–373. [PubMed: 9044906]
52. Issels RD, Abdel-Rahman S, Wendtner CM, Falk MH, Kurze V, Sauer H, Aydemir U, Hiddemann W. Neoadjuvant chemotherapy combined with regional hyperthermia (RHT) for locally advanced primary or recurrent high-risk adult soft-tissue sarcomas (STS) of adults: long-term results of a phase II study. Eur J Cancer. 2001; 37:1599–1608. [PubMed: 11527684]
53. Overgaard J, Gonzalez DG, Hulshof M, Arcangeli G, Dahl O, Mella O, Bentzen SM. Randomized Trial of Hyperthermia as Adjuvant to Radiotherapy for Recurrent or Metastatic Malignant-Melanoma. Lancet. 1995; 345:540–543. [PubMed: 7776772]
54. Rau B, Wust P, Hohenberger P, Loffel J, Hunerbein M, Below C, Gellermann J, Speidel A, Vogl T, Riess H, Felix R, Schlag PM. Preoperative hyperthermia combined with radiochemotherapy in locally advanced rectal cancer - A phase II clinical trial. Ann Surgery. 1998; 227:380–389.
55. Van Der Zee J, Gonzalez DG, Van Rhoon GC, Van Dijk JDP, Van Putten WLJ, Hart AAM. Comparison of radiotherapy alone with radiotherapy plus hyperthermia in locally advanced pelvic tumours: a prospective, randomised, multicentre trial. Lancet. 2000; 355:1119–1125. [PubMed: 10791373]
56. Vernon CC, Hand JW, Field SB, Machin D, Whaley JB, Vanderzee J, Vanputten WLJ, Vanrhoon GC, Vandijk JDP, Gonzalez DG, Liu FF, Goodman P, Sherar M. Radiotherapy with or without hyperthermia in the treatment of superficial localized breast cancer: Results from five randomized controlled trials. Int J Radiat Oncol Biol Phys. 1996; 35:731–744. [PubMed: 8690639]
57. Mckenziei AL, Carruth JAS. Lasers in surgery and medicine. Phys Med Biol. 1984; 29:619–641. [PubMed: 6235527]
58. Svaasand LO, Gomer CJ, Morinelli EA. On the physical rationale of laser induced hyperthermia. Lasers Med Sci. 1990; 5:121–128.
59. Brunetaud JM, Mordon S, Maunoury V, Beacco C. Non-PDT uses of lasers in oncology. Lasers Med Sci. 1995; 10:3–8.
60. Chen WR, Adams RL, Bartels KE, Nordquist RE. Chromophore-Enhanced in-Vivo Tumor-Cell Destruction Using an 808-Nm Diode-Laser. Cancer Lett. 1995; 94:125–131. [PubMed: 7634239]
61. Chen WR, Adams RL, Carubelli R, Nordquist RE. Laser-photosensitizer assisted immunotherapy: A novel modality for cancer treatment. Cancer Lett. 1997; 115:25–30. [PubMed: 9097975]
62. Chen WR, Adams RL, Higgins AK, Bartels KE, Nordquist RE. Photothermal effects on murine mammary tumors using indocyanine green and an 808-nm diode laser: An in vivo efficacy study. Cancer Lett. 1996; 98:169–173. [PubMed: 8556705]
63. Dolmans D, Fukumura D, Jain RK. Photodynamic therapy for cancer. Nat Rev Cancer. 2003; 3:380–387. [PubMed: 12724736]
64. Dougherty TJ, Gomer CJ, Henderson BW, Jori G, Kessel D, Korbelik M, Moan J, Peng Q. Photodynamic therapy. J Nat Cancer Inst. 1998; 90:889–905. [PubMed: 9637138]
65. Henderson BW, Dougherty TJ. How Does Photodynamic Therapy Work. J Photochem Photobiol. 1992; 55:145–157.
66. Elisseeff J, Anseth K, Sims D, Mcintosh W, Randolph M, Langer R. Transdermal photopolymerization for minimally invasive implantation. Proc Natl Acad Sci USA. 1999; 96:3104–3107. [PubMed: 10077644]
67. Murphy CJ, San TK, Gole AM, Orendorff CJ, Gao JX, Gou L, Hunyadi SE, Li T. Anisotropic metal nanoparticles: Synthesis, assembly, and optical applications. J Phys Chem B. 2005; 109:13857–13870. [PubMed: 16852739]
68. Nikoobakht B, El-Sayed MA. Preparation and growth mechanism of gold nanorods (NRs) using seed-mediated growth method. Chem Mat. 2003; 15:1957–1962.
69. Wiley B, Sun Y, Xia Y. Synthesis of Silver Nanostructures with Controlled Shapes and Properties. Acc Chem Res. 2007; 40:1067–1076. [PubMed: 17616165]

70. Huang X, Jain PK, El-Sayed IH, El-Sayed MA. Plasmonic photothermal therapy using gold nanoparticles. Lasers Med Sci ASAP. 2007
71. Huang X, El-Sayed IH, Qian W, El-Sayed MA. The potential use of the enhanced nonlinear properties of gold nanospheres in photothermal cancer therapy. Lasers Surg & Med. 2007; 39:747–753. [PubMed: 17960762]
72. Huff TB, Tong L, Zhao Y, Hansen MN, Cheng JX, Wei A. Hyperthermic effects of gold nanorods on tumor cells. Nanomedicine. 2007; 2:125–132. [PubMed: 17716198]
73. Hu M, Chen JY, Li ZY, Au L, Hartland GV, Li XD, Marquez M, Xia YN. Gold nanostructures: engineering their plasmonic properties for biomedical applications. Chem Soc Rev. 2006; 35:1084–1094. [PubMed: 17057837]
74. Gans R. Form of ultramicroscopic particles of silver. Ann Phys. 1915; 47:270–284.
75. Gole A, Murphy CJ. Seed-mediated synthesis of gold nanorods: Role of the size and nature of the seed. Chem Mat. 2004; 16:3633–3640.
76. Perez-Juste J, Pastoriza-Santos I, Liz-Marzan LM, Mulvaney P. Gold nanorods: Synthesis, characterization and applications. Coord Chem Rev. 2005; 249:1870–1901.
77. Harris JM, Chess RB. Effect of pegylation on pharmaceuticals. Nat Rev Drug Discov. 2003; 2:214–221. [PubMed: 12612647]
78. Huff TB, Hansen MN, Zhao Y, Cheng JX, Wei A. Controlling the cellular uptake of gold nanorods. Langmuir. 2007; 23:1596–1599. [PubMed: 17279633]
79. Liao HW, Hafner JH. Gold nanorod bioconjugates. Chem Mat. 2005; 17:4636–4641.
80. Niidome T, Yamagata M, Okamoto Y, Akiyama Y, Takahashi H, Kawano T, Katayama Y, Niidome Y. PEG-modified gold nanorods with a stealth character for in vivo applications. J Control Release. 2006; 114:343–347. [PubMed: 16876898]
81. Maeda H. The enhanced permeability and retention (EPR) effect in tumor vasculature: The key role of tumor-selective macromolecular drug targeting. Adv Enzyme Regul. 2001; 41:189–207. [PubMed: 11384745]
82. Jain RK. Transport of Molecules in the Tumor Interstitium: A Review. Cancer Res. 1987; 47:3039–3051. [PubMed: 3555767]
83. Li GC, Mivechi NF, Weitzel G. Heat-Shock Proteins, Thermotolerance, and Their Relevance to Clinical Hyperthermia. Int J Hyperthermia. 1995; 11:459–488. [PubMed: 7594802]
84. Borrelli MJ, Wong RSL, Dewey WC. A Direct Correlation between Hyperthermia-Induced Membrane Blebbing and Survival in Synchronous G1 Cho Cells. J Cell Physiol. 1986; 126:181–190. [PubMed: 3944204]
85. Coleman ML, Sahai EA, Yeo M, Bosch M, Dewar A, Olson MF. Membrane blebbing during apoptosis results from caspase-mediated activation of ROCK I. Nat Cell Biol. 2001; 3:339–345. [PubMed: 11283606]
86. Sebbagh M, Renvoize C, Hamelin J, Riche N, Bertoglio J, Breard J. Caspase-3-mediated cleavage of ROCK I induces MLC phosphorylation and apoptotic membrane blebbing. Nat Cell Biol. 2001; 3:346–352. [PubMed: 11283607]
87. Mills JC, Stone NL, Erhardt J, Pittman RN. Apoptotic membrane blebbing is regulated by myosin light chain phosphorylation. J Cell Biol. 1998; 140:627–636. [PubMed: 9456322]
88. Kowal-Vern A, Mcgill V, Walenga JM, Gamelli RL. Antithrombin III concentrate in the acute phase of thermal injury. Burns. 2000; 26:97–101. [PubMed: 10630326]

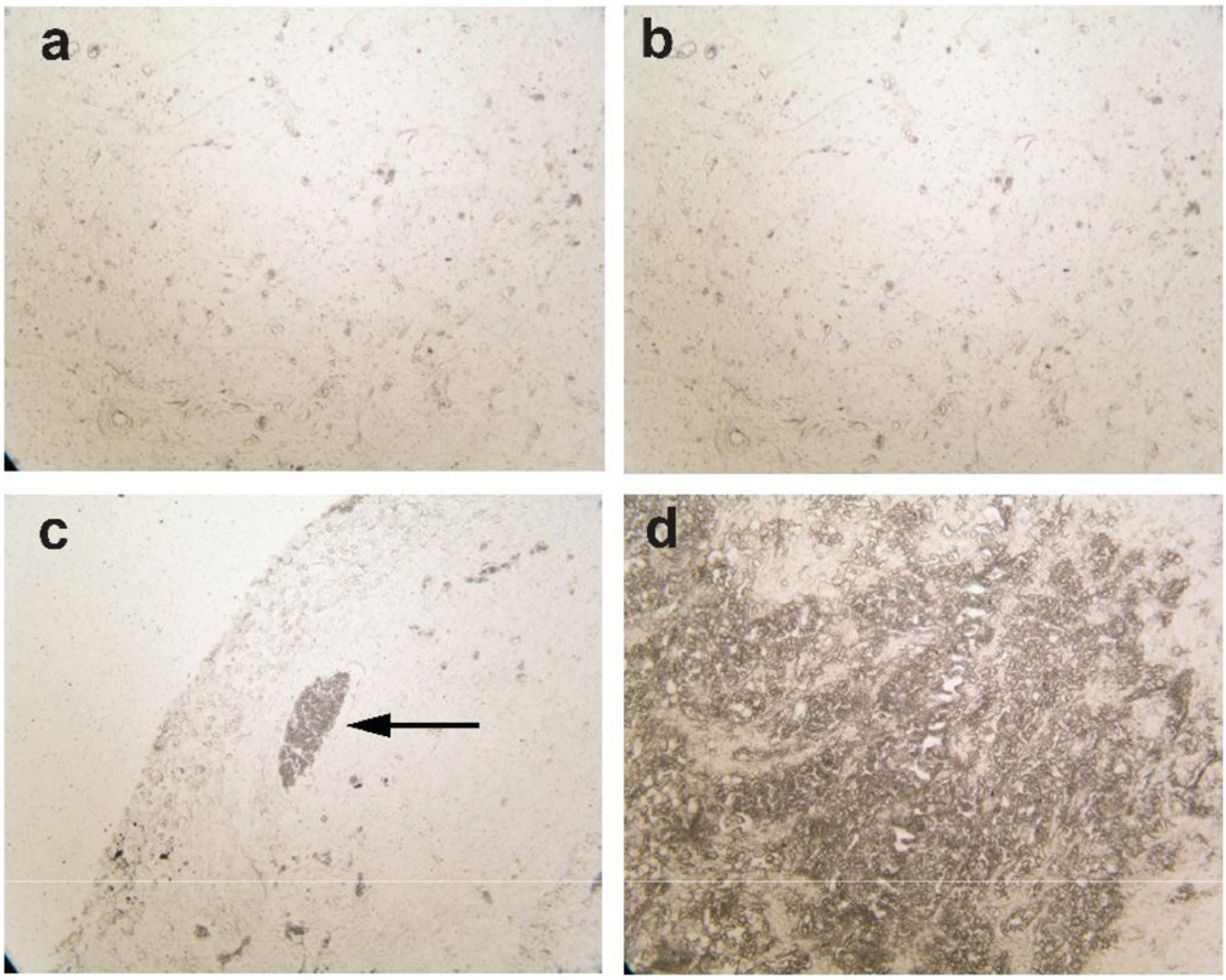

Fig. 1.

Histological sections of silver stained HSC-3 tumor xenografts from female *nu/nu* mice intravenously (tail) injected with (a) 100 μL of 10 mM PBS following 24 hr circulation and pegylated gold nanorods (100 μL, $OD_{\lambda=800}$=120) following (b) 2 hr (c), 6 hr, and (d) 24 hr accumulation. Direct injection of particles to the tumor interstitium was used as a positive staining control (data not shown). Arrow indicates staining of red blood cells (observed in all tumors).

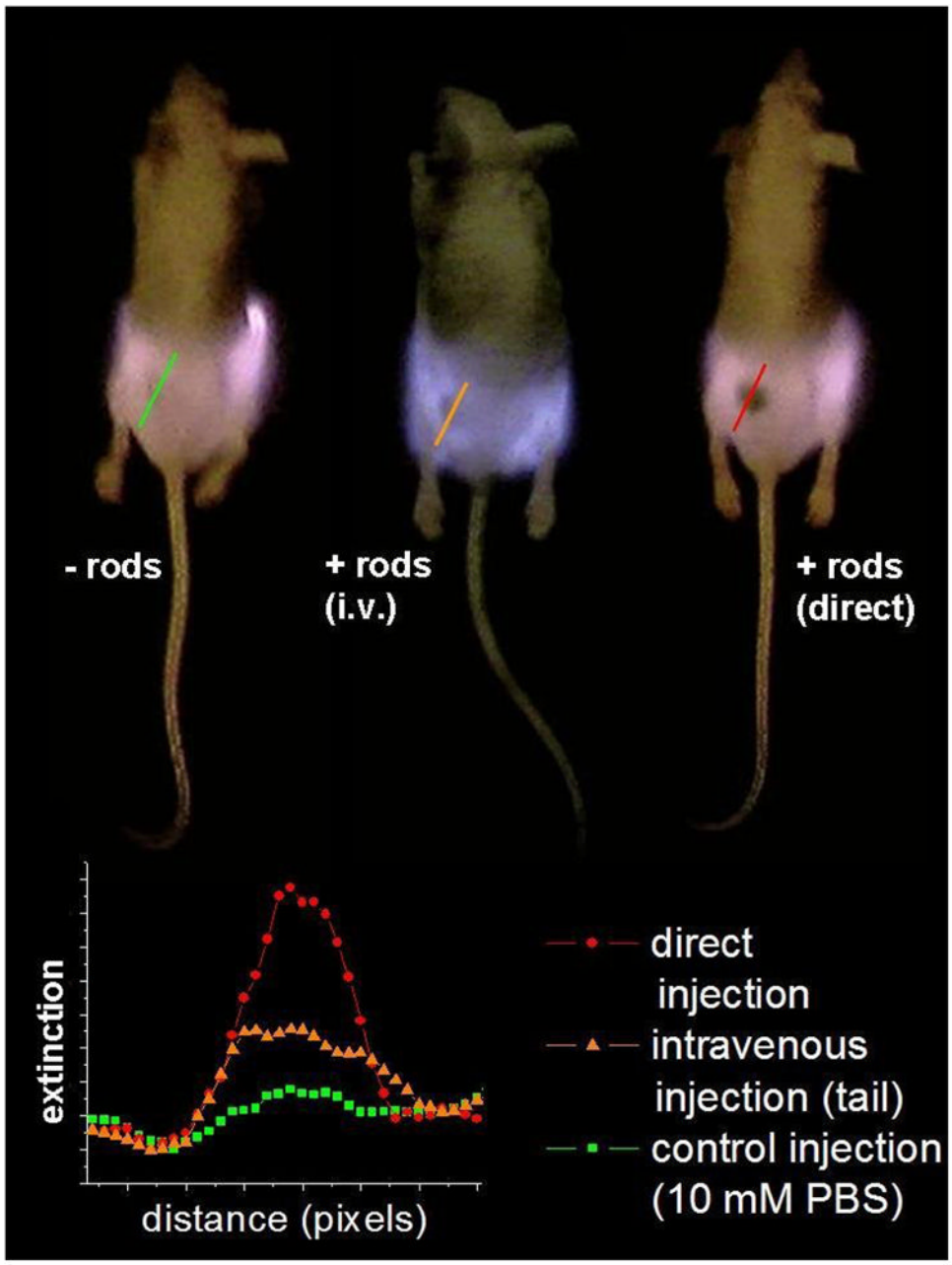

Fig. 2.

NIR transmission images of mice prior to PPTT treatments. Inset shows intensity line-scans of NIR extinction at tumor sites for control (■), intravenous (▲), and direct (●) administration of pegylated gold nanorods. Control mice were interstitially injected with 15 μL 10 mM PBS alone, while directly administered mice received interstitial injections of 15 μL pegylated gold nanorods ($OD_{\lambda=800}$=40, 2 min accumulation), and intravenously administered mice recieved 100 μL pegylated gold nanorod ($OD_{\lambda=800}$=120, 24 hr accumulation) injections.

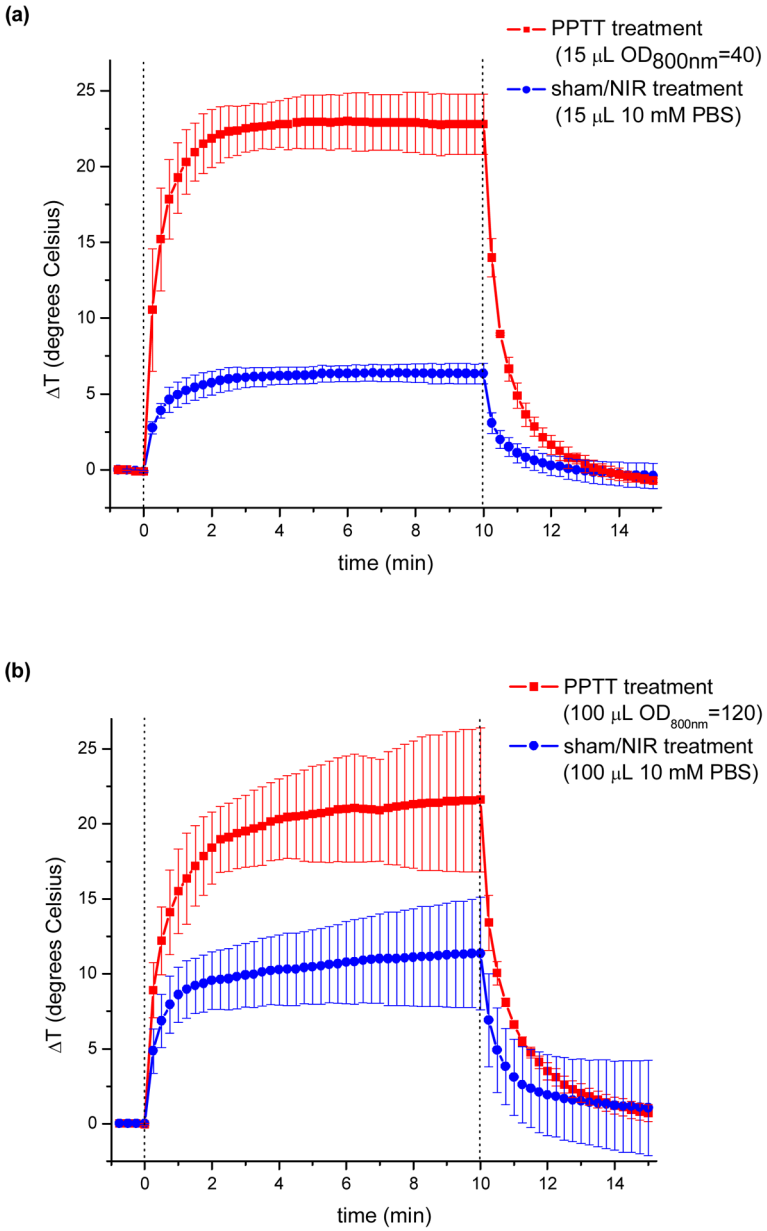

Fig. 3.

Thermal transient measurements of HSC-3 tumor interstitia during (a) direct and (b) intravenous near-infrared PPTT (■) and sham/NIR (●) treatments using pegylated gold nanorods. Direct PPTT treatments were performed by administration of 15 μL pegylated gold nanorods ($OD_{\lambda=800}$=40, 2 min accumulation) followed by 10 min of 0.9–1.1 W/cm^2 NIR laser exposure. Intravenous PPTT treatments were performed by administration of 100 μL pegylated gold nanorods ($OD_{\lambda=800}$=120, 24 hr accumulation) followed by 10 min of 1.7–1.9 W/cm^2 NIR laser exposure. Sham/NIR treatments were performed by administration of 15 μL 10 mM PBS and NIR laser exposure of comperable time and power density. Errors reported as standard deviation.

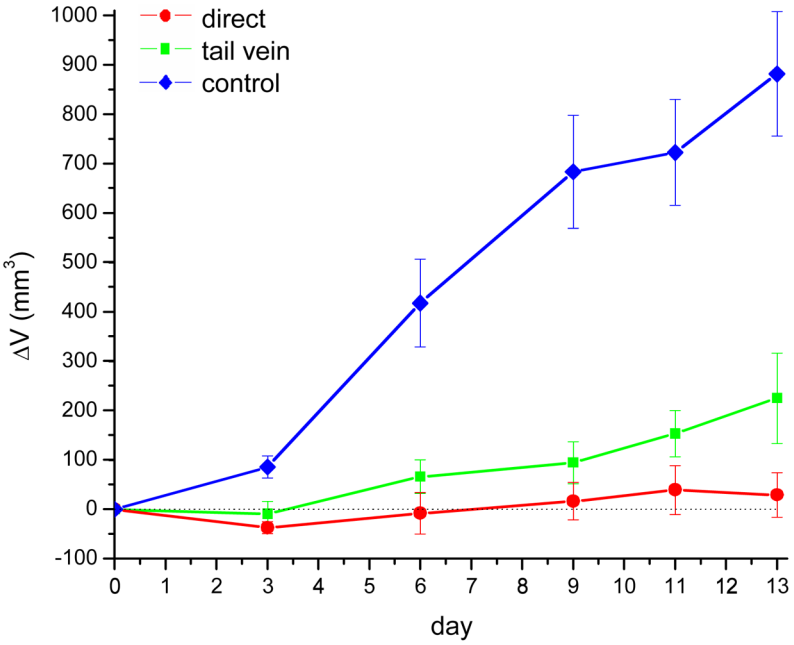

Fig. 4.

Average change in tumor volume for HSC-3 xenografts following near-infrared PPTT treatment by control (♦), intravenous (■), and direct (●) injection of pegylated gold nanorods. Errors for control (n=10), direct injection (n=8), and intravenous injection (n=7) groups reported as standard error of the means. Control mice were treated by interstitial injection of 15 μL 10 mM PBS alone, while intravenous PPTT treatments were performed by administration of 100 μL pegylated gold nanorods ($OD_{\lambda=800}$=120, 24 hr accumulation) followed by 10 min of 1.7–1.9 W/cm^2 NIR laser exposure. Direct PPTT treatments were performed by administration of 15 μL pegylated gold nanorods ($OD_{\lambda=800}$=40, 2 min accumulation) followed by 10 min of 0.9–1.1 W/cm^2 NIR laser exposure.

Table I

P-values for average volume change in HSC-3 tumors following near-infrared PPTT by 808 nm irradiation of pegylated gold nanorods.

	day 0	day 3	day 6	day 9	day 11	day 13
direct vs control	-	0.0003	0.001	0.0002	0.0001	0.0001
tail vein vs control	-	0.0136	0.0037	0.0005	0.0004	0.0008
direct vs tail	-	0.3415	0.1896	0.1936	0.1205	0.084

Table II

Non-parametric analysis of variance for near-infrared PPTT treatment (2) and control groups.

day 0	day 3	day 6	day 9	day 11	day 13
-	0.0024	0.0009	0.0008	0.0001	0.0005